Instituto de Física
Universidade de São Paulo

Toward a global description of the nucleus-nucleus interaction

Chamon, L.C.[1]; Carlson, B.V.[2]; Gasques, L.R.[1]; Pereira, D.[1]; De Conti, C.[2]; Alvarez, M.A.G.[1]; Hussein, M.S.[1]; Cândido Ribeiro, M.A.[3]; Rossi Jr., E.S.[1]; Silva, C.P.[1]

[1] Departamento de Física Nuclear, Instituto de Física da Universidade de São Paulo Caixa Postal 66318, 05315-970, São Paulo, SP,Brazil

[2] Departamento de Física, Instituto Tecnológico de Aeronáutica, Centro Técnico Aeroespacial, São José dos Campos, SP,Brazil

[3] Departamento de Física, Instituto deBiociências, Letras e Ciências Exatas, Universidade Estadual Paulista, São José do Rio Preto, SPBrazil

Publicação IF - 1537/2002

Toward a global description of the nucleus-nucleus interaction.

L. C. Chamon[1], B. V. Carlson[2], L. R. Gasques[1], D. Pereira[1], C. De Conti[2], M. A. G. Alvarez[1], M. S. Hussein[1], M. A. Cândido Ribeiro[3], E. S. Rossi Jr.[1] and C. P. Silva[1].

1. Departamento de Física Nuclear, Instituto de Física da Universidade de São Paulo, Caixa Postal 66318, 05315-970, São Paulo, SP, Brazil.

2. Departamento de Física, Instituto Tecnológico de Aeronáutica, Centro Técnico Aeroespacial, São José dos Campos, SP, Brazil.

3. Departamento de Física, Instituto de Biociências, Letras e Ciências Exatas, Universidade Estadual Paulista, São José do Rio Preto, SP, Brazil.

Extensive systematizations of theoretical and experimental nuclear densities and of optical potential strengths extracted from heavy-ion elastic scattering data analyses at low and intermediate energies are presented. The energy-dependence of the nuclear potential is accounted for within a model based on the nonlocal nature of the interaction. The systematics indicates that the heavy-ion nuclear potential can be described in a simple global way through a double-folding shape, which basically depends only on the density of nucleons of the partners in the collision. The possibility of extracting information about the nucleon-nucleon interaction from the heavy-ion potential is investigated.

PACS: 24.10.Ht, 13.75.Cs, 21.10.Ft, 21.10.Gv, 21.30.-x
Keywords: Heavy-ion nuclear potential. Proton, neutron, charge, nucleon and matter density distributions. Effective nucleon-nucleon interaction.

1. Introduction

The optical potential plays a central role in the description of heavy-ion collisions, since it is widely used in studies of the elastic scattering process as well as in more complicated reactions through the DWBA or coupled-channel formalisms. This complex and energy-dependent potential is composed of the bare and polarization potentials, the latter containing the contribution arising from nonelastic couplings. In principle, the bare (or nuclear) potential between two heavy ions can be associated with the fundamental nucleon-nucleon interaction folded into a product of the nucleon densities of the nuclei [1]. Apart from some structure effects, the shape of the nuclear density along the table of stable nuclides is nearly a Fermi distribution, with diffuseness approximately constant and radius given roughly by $R = r_0\, A^{1/3}$, where A is the number of nucleons of the nucleus. Therefore, one could expect a simple dependence of the heavy-ion nuclear potential on the number of nucleons of the partners in the collision. In fact, analytical formulae have been deduced [2–4] for the folding potential, and simple expressions have been obtained at the surface region. An universal (system-independent) shape for the heavy-ion nuclear potential has been derived [5] also in the framework of the liquid-drop model, from the Proximity Theorem which relates the force between two nuclei to the interaction between flat surfaces made of semi-infinite nuclear matter. The theorem leads [5] to an expression for the potential in the form of a product of a geometrical factor by a function of the separation between the surfaces of the nuclei.

The elastic scattering is the simplest process that occurs in a heavy-ion collision because it involves very litle rearrangement of matter and energy. Therefore, this process has been studied in a large number of experimental investigations, and a huge body of elastic cross section data is currently available. The angular distribution for elastic scattering provides unambiguous determination of the real part of the optical potential only in a region around a particular distance [6] hereafter referred as the sensitivity radius (R_S). At energies close to the Coulomb barrier the sensitivity radius is situated in the surface region. In this energy region, the systematization [7,8] of experimental results for potential strengths at the sensitivity radii has provided an universal exponential shape for the heavy-ion nuclear potential at the surface, as theoretically expected, but with a diffuseness value smaller than that originally proposed in the proximity potential.

In a recent review article [6] the phenomenon of rainbow scattering was discussed, and it was emphasized that the real part of the optical potential can be unambiguously extracted also at very short distances from heavy-ion elastic scattering data at intermediate energies. Such a kind of data has been first obtained for α-particle scattering from a variety of nuclei over a large range of energies [9–11], and later for several heavy-ion systems. However, differently from the case for the surface region (low energy), a systematization of potential strengths at the inner distances has not

been performed up to now, probably because the resulting phenomenological interactions have presented significant dependence on the bombarding energies. Several theoretical models have been developed to account for this energy-dependence through realistic mean field potentials. Most of them are improvements of the original double-folding potential with the nucleon-nucleon interaction assumed to be energy- and density-dependent [6]. Another recent and successful model [12–14] associates the energy-dependence of the heavy-ion bare potential with nonlocal quantum effects related to the exchange of nucleons between target and projectile, resulting in a very simple expression for the energy-dependence of the nuclear potential. Using the model of Refs. [12–14], in the present work we have realized a systematization of potential strengths extracted from elastic scattering data analyses, considering both: low (near-barrier) and intermediate energies. The systematics indicates that the heavy-ion nuclear potential can be described in a simple global way through a double-folding shape, which basically depends only on the number of nucleons of the nuclei.

The paper is organized as follows. In Section 2, as a preparatory step for the potential systematization, an extensive and systematic study of nuclear densities is presented. This study is based on charge distributions extracted from electron scattering experiments [15,16] as well as on theoretical densities derived from the Dirac-Hartree-Bogoliubov model [17]. In Section 3, analytical expressions for the double-folding potential are derived for the whole (surface and inner) interaction region, and a survey of the main characteristics of this potential is presented. Section 4 contains the nonlocal model for the heavy-ion bare interaction, including several details that have not been published before. Section 5 is devoted to the nuclear potential systematics. In Section 6, we discuss the role played by the nucleon-nucleon interaction, and we present, in a somewhat speculative way, an alternative form for the effective nucleon-nucleon interaction, which is consistent with our results for the heavy-ion nuclear potential. Finally, Section 7 contains a brief summary and the main conclusions.

2. Systematization of the nuclear densities

According to the double-folding model, the heavy-ion nuclear potential depends on the nuclear densities of the nuclei in collision. Thus, a systematization of the potential requires a previous systematization of the nuclear densities. In this work, with the aim of describing the proton, neutron, nucleon (proton+neutron), charge and matter densities, we adopt the two-parameter Fermi (2pF) distribution, which has also been commonly used for charge densities extracted from electron scattering experiments [15]. The shape, Eq. 1 and Fig. 1, of this distribution is particularly appealing for the density description, due to the flatness of the inner region, that is associated with the saturation of the nuclear medium, and to the rapid fall-off (related to the diffuseness parameter a) that brings out the notion of the radius, R_0, of the nucleus.

$$\rho(r) = \frac{\rho_0}{1 + exp\left(\frac{r - R_0}{a}\right)} \tag{1}$$

The ρ_0, a and R_0 parameters are connected by the normalization condition:

$$4\pi \int_0^\infty \rho(r)\, r^2\, dr = X\ , \tag{2}$$

where X could be the number of protons Z, neutrons N or nucleons $A = N + Z$. In our theoretical calculations, the charge distribution (ρ_{ch}) has been obtained by folding the proton distribution of the nucleus (ρ_p) with the intrinsic charge distribution of the proton in free space (ρ_{chp})

$$\rho_{ch}(r) = \int \rho_p(\vec{r'})\, \rho_{chp}(\vec{r} - \vec{r'})\, d\vec{r'}\ , \tag{3}$$

where ρ_{chp} is an exponential with diffuseness $a_{chp} = 0.235\ fm$. In an analogous way, we have defined the matter density of the nucleus by folding the nucleon distribution of the nucleus with the intrinsic matter distribution of the nucleon, which is assumed to have the same shape of the intrinsic charge distribution of the proton. For convenience, the charge and matter distributions are normalized to the number of protons and nucleons, respectively.

In order to systematize the heavy-ion nuclear densities, we have calculated theoretical distributions for a large number of nuclei using the Dirac-Hartree-Bogoliubov (DHB) model [17]. The DHB calculations were performed using the NL3 parameter set [18]. This set was obtained by adjusting the masses, and the charge and neutron radii of 10 nuclei in the region of the valley of stability, ranging from ^{16}O to ^{214}Pb, using the Dirac-Hartree-BCS (DH-BCS) model. For the cases in which they have been performed, calculations using this parameter set and either the DHB [17] or the DH-BCS [18–20] model have shown very good agreement with experimental masses and radii. In the present

work, we have also used the results of previous systematics for charge distributions [15,16], extracted from electron scattering experiments, as a further check of our DHB results. All the theoretical and most of the "experimental" densities are not exact Fermi distributions. Thus, with the aim of studying the equivalent diffuseness of the densities, we have calculated the corresponding logarithmic derivatives (Eq. 4) at the surface region (at $r \approx R_0 + 2\ fm$).

$$a \approx -\frac{\rho(r)}{\frac{d\rho}{dr}} \tag{4}$$

Fig. 2a shows the results for the experimental charge distributions: the diffuseness values spread around an average diffuseness $\bar{a}_c = 0.53\ fm$, with standard deviation 0.04 fm. Most of this dispersion arises from experimental errors. Indeed, we have verified that different analyses (different electron scattering data set or different models for the charge density) for a given nucleus provide diffuseness values that differ from each other by about 0.03 fm. Therefore, the experimental charge distributions are compatible, within the experimental precision, with a constant diffuseness value. The theoretical charge distributions present similar behavior (Fig. 2b), with average value slightly smaller than the experimental one. In this case, the observed standard deviation, 0.02 fm, is associated with the effects of the structure of the nuclei. Despite the trend presented by the neutron and proton diffuseness (Fig. 2c), all the nucleon distributions result in very similar diffuseness values ($\bar{a}_N = 0.48\ fm$), with standard deviation 0.025 fm. Due to the folding procedure, the matter distributions present diffuseness values significantly greater ($\bar{a}_M = 0.54\ fm$) than those for the nucleon distributions. Taking into account that the theoretical calculations have slightly underestimated the experimental charge diffuseness, we consider that more realistic average values for the nucleon and matter density diffuseness are 0.50 fm and 0.56 fm, respectively. A dispersion (σ_a) of about 0.025 fm around these average values is expected due to effects of the structure of the nuclei.

The root-mean-square (RMS) radius of a distribution is defined by Eq. 5:

$$r_{rms} = \sqrt{\frac{\int r^2\ \rho(r)\ d\vec{r}}{\int \rho(r)\ d\vec{r}}}. \tag{5}$$

We have determined the radii R_0 for the 2pF distributions assuming that the corresponding RMS radii should be equal to those of the experimental (electron scattering) and theoretical (DHB) densities. The results for R_0 from theoretical charge distributions (Fig. 3b) are very similar to those from electron experiments (Fig. 3a). This fact indicates that the radii obtained through the theoretical DHB calculations are quite realistic. The nucleon and matter densities give very similar radii (Fig. 3d), which are well described by the following linear fit:

$$R_0 = 1.31\ A^{1/3} - 0.84\ fm. \tag{6}$$

Due to effects of the structure of the nuclei, the R_0 values spread around this linear fit with dispersion $\sigma_{R_0} = 0.07\ fm$, but the heavier the nucleus is, the smaller is the deviation. In Fig. 4 are shown the theoretical (DHB) nucleon densities for a few nuclei, and the corresponding 2pF distributions with $a = 0.50\ fm$ and R_0 values obtained from Eq. 6.

3. Essential features of the folding potential

The double-folding potential has the form

$$V_F(R) = \int \rho_1(r_1)\ \rho_2(r_2)\ v_{NN}(\vec{R} - \vec{r_1} + \vec{r_2})\ d\vec{r_1}\ d\vec{r_2}\ , \tag{7}$$

where R is the distance between the centers of the nuclei, ρ_i are the respective nucleon distributions, and $v_{NN}(\vec{r})$ is the effective nucleon-nucleon interaction. The success of the folding model can only be judged meaningfully if the effective nucleon-nucleon interaction employed is truly realistic. The most widely used realistic interaction is known as M3Y [1,6], which can usually assume two versions: Reid and Paris.

For the purpose of illustrating the effects of density variations on the folding potential, we show in Fig. 5 the results obtained for different sets of 2pF distributions. In Section 2, we have estimated the dispersions of the R_0 and a parameters, $\sigma_{R_0} \approx 0.07$ and $\sigma_a \approx 0.025\ fm$, that arise from effects of the structure of the nuclei. Observe that these standard deviations are one half of the corresponding variations considered in the example of Fig. 5, $\Delta R_0 = 0.14\ fm$ and $\Delta a = 0.05\ fm$. The surface region of the potential ($R \geq R_1 + R_2$) is much more sensitive to small changes of the density parameters than the inner region. Our calculations indicate that, due to such structure effects, the strength of the nuclear potential in the region near the barrier radius may vary by about 20%, and the major part of this

variation is connected to the standard deviation of the parameter a. Therefore, concerning the nuclear potential, the effects of the structure of the nuclei are mostly present at the surface and mainly related to the diffuseness parameter.

The six-dimensional integral (Eq. 7) can easily be solved by reducing it to a product of three one-dimensional Fourier transforms [1], but the results may only be obtained through numerical calculations. In order to provide analytical expressions for the folding potential, we consider, as an approximation, that the range of the effective nucleon-nucleon interaction is negligible in comparison with the diffuseness of the nuclear densities. In this zero-range approach, the double-folding potential can be obtained from:

$$v_{NN}(\vec{r}) \approx V_0\,\delta(\vec{r}) \Rightarrow V_F(R) = \frac{2\pi V_0}{R}\int_0^\infty r_1\,\rho_1(r_1)\left[\int_{|R-r_1|}^{R+r_1} r_2\,\rho_2(r_2)\,dr_2\right]dr_1. \tag{8}$$

As discussed in Section 2, the heavy-ion densities involved in Eq. 8 are approximately 2pF distributions, with $R_0 \gg a$. In the limit $a \to 0$, the double-integral results in

$$V_F(R \leq R_2 - R_1) = V_0\,\rho_{01}\,\rho_{02}\,\frac{4}{3}\pi R_1^3\,, \tag{9}$$

$$V_F(R_2 - R_1 \leq R \leq R_1 + R_2) = V_0\,\rho_{01}\,\rho_{02}\,\frac{4}{3}\pi\mathcal{R}^3\left(\frac{\tau^2}{1+\zeta\tau}\right)\left[\frac{3}{8} + \frac{\tau}{4} + \zeta\frac{\tau^2}{16}\right]\,, \tag{10}$$

$$V_F(R \geq R_1 + R_2) = 0\,, \tag{11}$$

where $s = R - (R_1 + R_2)$, $\mathcal{R} = 2R_1R_2/(R_1 + R_2)$, $\zeta = \mathcal{R}/(R_1 + R_2)$, $\tau = s/\mathcal{R}$, R_1 and R_2 are the radii of the nuclei (hereafter we consider $R_2 \geq R_1$). We need a further approximation to obtain analytical expressions for the folding potential in the case of finite diffuseness value.

The Fermi distribution may be represented, with precision better than 3% for any r value (see Fig. 1), by:

$$\frac{\rho_0}{1 + exp\left(\frac{r-R_0}{a}\right)} \approx \rho_0\,C\left(\frac{r - R_0}{a}\right)\,, \tag{12}$$

$$C(x \leq 0) = 1 - \frac{7}{8}e^x + \frac{3}{8}e^{2x}\,, \tag{13}$$

$$C(x \geq 0) = e^{-x}\left(1 - \frac{7}{8}e^{-x} + \frac{3}{8}e^{-2x}\right). \tag{14}$$

This approximation is particularly useful in obtaining analytical expressions for integrals that involve the 2pF distribution. If both nuclei have the same diffuseness a, the double-integral (Eq. 8) can be solved analytically using the approximation represented by Eq. 12, and the result expressed as a sum of a large number of terms, most of them negligible for $a \ll R_0$. Rather simple expressions can be found after an elaborate algebraic manipulation:

$$V_F(R \leq R_2 - R_1 + a) \approx V_0\,\rho_{01}\,\rho_{02}\,\frac{4}{3}\pi R_1^3\left\{1 + 9.7\left(\frac{a}{R_1}\right)^2 - \left[0.875\left(\frac{R_2^3}{R_1^3} - 1\right) + \frac{a}{R_1}\left(2.4 + \frac{R_2^2}{R_1^2}\right)\right]e^{-(R_2-R_1)/a}\right\}\,, \tag{15}$$

$$V_F(R_2 - R_1 + a \leq R \leq R_1 + R_2) \approx V_0\,\rho_{01}\,\rho_{02}$$
$$\frac{4}{3}\pi\mathcal{R}^3\left(\frac{1}{1+\zeta\tau}\right)\left\{\tau^2\left[\frac{3}{8} + \frac{\tau}{4} + \zeta\frac{\tau^2}{16}\right] + 2.4\,\eta^2\left[1 - \frac{5}{8}\eta - \zeta\tau^2 + \left(\frac{5}{4}\eta - \frac{1}{2}\right)e^{\varepsilon} + \left(1 + \frac{5}{8}\eta\right)e^{-(\varepsilon+2R_1/a)}\right]\right\}\,, \tag{16}$$

$$V_F(R \geq R_1 + R_2) \approx V_0\,\rho_{01}\,\rho_{02}\,\pi a^2\,\mathcal{R}\,g(\tau)\,f(s/a)\,, \tag{17}$$

with $\eta = a/\mathcal{R}$, $\varepsilon = s/a$. The functions g and f are given by:

$$g(\tau) = \frac{1+\tau+\tau^2\zeta/3+\eta+(\eta+1/2)\,e^{-\varepsilon}}{1+\zeta\tau}\,, \tag{18}$$

$$f(s/a) = (1+s/a)\,e^{-s/a}\,. \tag{19}$$

If the nuclei have slightly (about 10%) different diffuseness, the formulae are still valid with $a \approx (a_1+a_2)/2$. As an example of the precision of the analytical expressions above, we exhibit in Fig. 6 the results of numerical calculations (Eq. 8) and compare them with those from Eqs. 15, 16 and 17, and also with the exact expressions for $a = 0$, Eqs. 9, 10 and 11.

Eq. 17 presents some similarity with the proximity potential [5]:

$$V_P = 2\pi\Gamma\mathcal{R}d\,\Phi(s/d)\,, \tag{20}$$

where d is the "surface width", and Φ is an universal (system-independent) function. For a 2pF distribution, the surface width is related to the diffuseness parameter through: $d \approx (\pi/\sqrt{3})\,a$ [21]. The theoretical value adopted for d is 1 fm [5], which corresponds to a diffuseness $a \approx 0.55\ fm$. Taking into account that the Γ value is rather system-independent [5], systematizations of heavy-ion potential strengths extracted from elastic scattering data analyses have been performed by using the following expression, which should be valid for surface distances,

$$\frac{V_P(s \gg 0)}{\mathcal{R}} = V_0\,e^{-s/\alpha}\,. \tag{21}$$

The resulting experimental α values are quite similar, $\alpha \approx 0.62\ fm$ [7,8], but smaller than the theoretical prediction of the proximity potential $\alpha \approx 0.75\ fm$ [5]. Such systematics have included only experimental potential strengths in the surface region, in contrast to the case of the proximity potential where $V/\mathcal{R}$ should be an universal function of s also for inner distances. The proximity potential is not fully agreeing with our results for the double-folding potential in the zero-range approach (see Fig. 7). In fact, Eq. 17 indicates that a better choice for an universal quantity at the surface region would be

$$V_{red}(s \geq 0) = \frac{V_F}{\rho_{01}\,\rho_{02}\,\pi a^2\mathcal{R}\,g(\tau)}\,, \tag{22}$$

which results (from Eqs. 17, 19 and 22) the system-independent expression

$$V_{red}(s \geq 0) \approx V_0\,(1+s/a)\,e^{-s/a}\,. \tag{23}$$

However, it is not clear that one can find a simple form for such a universal quantity at inner distances from Eqs. 15 and 16. In Section 5, the reduced potential, V_{red}, is useful for addressig the potential strength systematization. Thus we define V_{red} for $s \leq 0$ through the following trivial form:

$$V_{red}(s \leq 0) = V_0\,. \tag{24}$$

The end of this section is devoted to the study of the effect on the folding potential of a finite range for the effective nucleon-nucleon interaction. The tri-dimensional delta function, $V_0\,\delta(\vec{r})$, can be represented through the limit $\sigma \to 0$ applied to the finite-range Yukawa function

$$Y_\sigma(r) = V_0\,\frac{e^{-r/\sigma}}{4\pi r\sigma^2}\,. \tag{25}$$

Fig. 8 shows a comparison of folding potentials in the zero-range approach (Eq. 8) with the result obtained (from Eq. 7) using an Yukawa function for the effective nucleon-nucleon interaction. The finite range is not truly significant at small distances, and can be accurately simulated at the surface, within the zero-range approach, just by slightly increasing the diffuseness of the nuclear densities.

4. A nonlocal description of the nucleus-nucleus interaction

Before proceeding with the systematization of the potential, we first set the stage for the model of the heavy-ion nuclear interaction [12–14]. When dealing with nonlocal interactions, one is required to solve the following integro-differential equation

$$-\frac{\hbar^2}{2\mu}\nabla^2\Psi(\vec{R}) + [V_C(R) + V_{pol}(R,E) + iW_{pol}(R,E)]\,\Psi(\vec{R}) + \int U(\vec{R},\vec{R}')\;\Psi(\vec{R}')\;d\vec{R}' = E\Psi(\vec{R})\;. \tag{26}$$

V_C is the Coulomb interaction assumed to be local. V_{pol} and W_{pol} are the real and imaginary parts of the polarization potential, and contain the contribution arising from nonelastic channel couplings. The corresponding nonlocality, called the Feshbach nonlocality, is implicit through the energy-dependence of these terms, consistent with the dispersion relation [22]. $U(\vec{R},\vec{R}')$ is the bare interaction and the nonlocality here, the Pauli nonlocality, is solely due to the Pauli exclusion principle and involves the exchange of nucleons between target and projectile.

Guided by the microscopic treatment of the nucleon-nucleus scattering [23–27], the following ansatz is assumed for the heavy-ion bare interaction [13]

$$U(\vec{R},\vec{R}') = V_{NL}\left(\frac{R+R'}{2}\right)\frac{1}{\pi^{3/2}b^3}e^{-\left(|\vec{R}+\vec{R}'|/b\right)^2}\;, \tag{27}$$

where b is the range of the Pauli nonlocality. Introduced in this way, the nonlocality is a correction to the local model, and in the $b \to 0$ limit Eq. 26 reduces to the usual Schröedinger differential equation. The range of the nonlocality can be found through $b \approx b_0 m_0/\mu$ [28], where $b_0 = 0.85\ fm$ is the nucleon-nucleus nonlocality parameter [23], m_0 is the nucleon mass, and μ is the reduced mass of the nucleus-nucleus system. This type of very mild nonlocality in the nucleon-nucleus and nucleus-nucleus interaction is to be contrasted with the very strong nonlocality found in the pion-nucleus interaction in the Δ-region [29]. In such cases, even the concept of an optical potential becomes dubious. In our case, however, we are on very safe ground.

The relation between the nonlocal interaction and the folding potential is obtained from [13]

$$V_{NL}(R) = V_F(R)\;. \tag{28}$$

Due to the central nature of the interaction, it is convenient to write down the usual expansion in partial waves,

$$\Psi(\vec{R}) = \sum i^\ell(2\ell+1)\frac{u_\ell(R)}{kR}\;P_\ell[cos(\theta)]\;, \tag{29}$$

$$U(\vec{R},\vec{R}') = \sum \frac{2\ell+1}{4\pi RR'}\;V_\ell(R,R')\;P_\ell[cos(\phi)]\;, \tag{30}$$

$$V_\ell(R,R') = V_{NL}\left(\frac{R+R'}{2}\right)\frac{1}{b\pi^{1/2}}\left[Q_\ell\left(\frac{2RR'}{b^2}\right)e^{-\left(\frac{R-R'}{b}\right)^2}(-)^{\ell+1}Q_\ell\left(\frac{-2RR'}{b^2}\right)e^{-\left(\frac{R+R'}{b}\right)^2}\right]\;, \tag{31}$$

where Q_ℓ are polynomials and ϕ is the angle between $\vec{R}$ and $\vec{R}'$ [23] . Thus, the integro-differential equation can be recast into the following form

$$\frac{\hbar^2}{2\mu}\frac{d^2u_\ell(R)}{dR^2} + \left[E - V_C(R) - V_{pol}(R,E) - iW_{pol}(R,E) - \frac{\ell(\ell+1)\hbar^2}{2\mu R^2}\right]u_\ell(R) = \int_0^\infty V_\ell(R,R')\;u_\ell(R')\;dR'\;. \tag{32}$$

When confronting theory and experiment, one usually relies on the optical model with a local potential. This brings into light the issue of extracting from Eq. 32 a local-equivalent (LE) potential

$$V_{LE}(R,E) + iW_{LE}(R,E) = \frac{1}{u_\ell(R)}\int_0^\infty V_\ell(R,R')\;u_\ell(R')\;dR'\;. \tag{33}$$

The presence of the wave-function in Eq. 33 indicates that the LE potential is complex and also ℓ- and energy-dependent. Despite its complex nature, the LE potential is not absorptive, $\langle\Psi|W_{LE}|\Psi\rangle = 0$; this statement can be demonstrated by considering that the nonlocal interaction is real and symmetrical, $V_\ell(R,R') = V_\ell(R',R)$. For neutron-nucleus systems, the LE potential is only weakly ℓ-dependent, and an approximate relation to describe its energy-dependence has been obtained [23]. A generalization of this relation for the ion-ion case is given by [12,13]:

$$V_{LE}(R,E) \approx V_F(R)\;e^{-\gamma[E-V_C(R)-V_{LE}(R,E)]}\;, \tag{34}$$

with $\gamma = \mu b^2/2\hbar^2$. In order to provide an example of the precision of expression 34, in Fig. 9 the corresponding result is compared to the exact LE potential (Eq. 33) obtained from the numerical resolution [13] of the respective

integro-differential equations (Eq. 32). The local-equivalent potential is quite well described by Eq. 34 for any ℓ value, except at very small distances ($R \approx 0$) that are not probed by heavy-ion experiments.

Expression 34 has accounted for the energy-dependence of experimentally extracted potential strengths for several systems in a very large energy range [12–14]. At near-barrier energies, $E \approx V_C(R_B) + V_{LE}(R_B)$, the effect of the Pauli nonlocality is negligible and $V_{LE}(R,E) \approx V_F(R)$, but the higher the energy is, the greater is the effect. At energies about 200 $MeV/nucleon$ the local-equivalent potential is about 1 order of magnitude less intense than the corresponding folding potential (see examples in Refs. [12,13]). In a classical physics framework, the exponent in Eq. 34 is related to the kinetic energy (E_k) and to the local relative speed between the nuclei (v) by

$$v^2 = \frac{2}{\mu} E_k(R) = \frac{2}{\mu} \left[E - V_C(R) - V_{LE}(R,E) \right] \; ; \tag{35}$$

and Eq. 34 may be rewritten in the following form

$$V_{LE}(R,E) \approx V_F(R) \; e^{-[m_0 b_0 v/(2\hbar)]^2} \approx V_F(R) \; e^{-4v^2/c^2} \; , \tag{36}$$

where c is the speed of light. Therefore, in this context the effect of the Pauli nonlocality is equivalent to a velocity-dependent nuclear interaction (Eq. 36). Another possible interpretation is that the local-equivalent potential may be associated directly with the folding potential (Eq. 37), with an effective nucleon-nucleon interaction (Eq. 38) dependent on the relative speed (v) between the nucleons

$$V_{LE}(R,E) = V_F = \int \rho_1(r_1) \; \rho_2(r_2) \; v_{NN}(v, \vec{R} - \vec{r_1} + \vec{r_2}) \; d\vec{r_1} \; d\vec{r_2} \; , \tag{37}$$

$$v_{NN}(v, \vec{r}) = v_f(\vec{r}) \; e^{-4v^2/c^2} \; . \tag{38}$$

5. The systematization of the nuclear potential

As already mentioned, the angular distribution for elastic scattering provides an unambiguous determination of the real part of the optical potential in a region around the sensitivity radius (R_S). For bombarding energies above (and near) the barrier, the sensitivity radius is rather energy-independent and close to the barrier radius (R_B), while at intermediate energies much inner distances are probed. At sub-barrier energies, the R_S is strongly energy-dependent, with its variation connected to the classical turning point; this fact has allowed the determination of the potential in a wide range of near-barrier distances, $R_B \leq R_S \leq R_B + 2 \; fm$. With the aim of avoiding ambiguities in the potential systematization, we have selected "experimental" (extracted from elastic scattering data analyses) potential strengths at the corresponding sensitivity radii, from works in which the R_S has been determined or at least estimated. In several articles, the authors claim that their data analyses at intermediate energies have unambiguously determined the nuclear potential in a quite extensive region of interaction distances. In such cases, we have considered potential strength "data" in steps of 1 fm over the whole probed region. Tables 1 and 2 provide the systems included in the nuclear potential systematics for the sub-barrier and intermediate energies, respectively. For the energy region above (and near) the barrier, the present systematics contains potential strengths for a large number of different heavy-ion systems from the previous Christensen and Winther's systematization [7]. Our systematics is not even near to being complete, but it is rather extensive and diversified enough to account well for the very large number of data that have been obtained in the last decades.

The experimental potential strengths represent the real part of the optical potential, which corresponds to the addition of the bare and polarization potentials. The contribution of the polarization to the optical potential depends on the particular features of the reaction channels involved in the collision, and is therefore quite system-dependent. If this contribution were very significant, it would be too difficult for one to set a global description of the heavy-ion nuclear interaction. In the present work, we neglect the real part of the polarization potential and associate the experimental potential strengths (V_{Exp}) with the bare interaction (V_{LE}). The success of our findings seems to support such a hypothesis.

In analysing experimental potential results for such a wide energy range and large number of different systems, we consider quite appropriate the use of system- and energy-independent quantities. We have removed the energy-dependence from the experimental potential strengths through the calculation of the corresponding folding potential strengths, V_{F-Exp}, based on Eq. 34. The system-dependence of the potential data set has then been removed with the use of the experimental reduced potential, $V_{red-Exp}$. For $s \geq 0$ this quantity was calculated from Eq. 22, and for inner s values we have adopted the following simple definition

$$V_{red-Exp} = V_0 \frac{V_{F-Exp}}{V_{F-Teo}} , \tag{39}$$

with V_{F-Teo} calculated through Eq. 8. The other useful quantity is the distance between surfaces: $s = R_S - (R_1 + R_2)$, where R_S is associated to the sensitivity radius, and the radii of the nuclei have been obtained from Eq. 6.

In Fig. 10 (top), the experimental reduced potential strengths are confronted with the theoretical prediction (Eqs. 23 and 24) for different diffuseness values. The fit to the data in the inner region ($s \leq 0$) results unambiguously in the value $V_0 = -456\ MeV\ fm^3$, and is quite insensitive to the diffuseness parameter, in agreement with the discussion about the folding features of Section 3. The fit for $s \geq 0$ is sensitive to both: V_0 and a, and the corresponding best fit values are $a = 0.56\ fm$ and the same V_0 found for the inner region. The standard deviation of the data set around the best fit (solid line in Fig. 10 - top) is 25%, a value somewhat greater than the dispersion (20%) expected to arise from effects of the structure of the nuclei (as discussed in Section 3). We believe that the remaining difference comes from two sources: uncertainties of the experimentally extracted potential strengths and the contribution of the polarization potential that we have neglected in our analysis. We point out that the best fit diffuseness value, $a = 0.56\ fm$, is equal to the average diffuseness found (Section 2) for the matter distributions and greater than the average value ($a = 0.50\ fm$) of the nucleon distributions. This is a consistent result because we have calculated the reduced potential strengths based on the zero-range approach (through Eqs. 8, 22, 23 and 24). As discussed in Section 3, the effect of a finite-range for the effective nucleon-nucleon interaction can be simulated, within the zero-range approach, by increasing the diffuseness of the (nucleon) densities of the nuclei. This subject is dealt with more deeply in the next Section.

In order to characterize the importance of the Pauli nonlocality, in Fig. 10 (bottom) are shown the results for the reduced potential through calculations performed without the correction (Eq. 34) due to the energy-dependence of the LE potential, i.e. associating the experimental potential strengths directly with the folding potential. The quality of the corresponding fit (Fig. 10 - bottom) is similar to that obtained with the nonlocality (Fig. 10 - top), but the V_0 and a parameters are significantly different. In the next Section, we show that the values found without considering the nonlocality, $a = 0.61\ fm$ and $V_0 = -274\ MeV\ fm^3$, seem to result in an unrealistic nucleon-nucleon interaction.

6. The effective nucleon-nucleon interaction

After removing the energy-dependence of the experimental potential strengths, the corresponding results are compatible with the double-folding potential in the zero-range approach (Eq. 8), provided that the matter densities of the nuclei be adopted in the folding procedure instead of the nucleon densities. In this section, we study the consistency of our results for the nuclear potential in the case that the double-folding model is treated in the more common interpretation: the nucleon distributions and a finite-range nucleon-nucleon interaction are assumed in Eq. 7. With the purpose of keeping the comparison between experimental and theoretical results through the use of system-independent quantities, it is necessary to change the definition of the experimental reduced potential

$$V_{red-Exp} = V_{red-Teo} \frac{V_{F-Exp}}{V_{F-Teo}} , \tag{40}$$

where V_{F-Teo} is now calculated through Eq. 7. $V_{red-Teo}$ is still obtained from Eqs. 23 and 24, with the V_0 parameter being associated to the volume integral of the effective nucleon-nucleon interaction (actually, this same procedure has also been adopted in the zero-range case)

$$V_0 = 4\pi \int v_{NN}(r)\, r^2\, dr . \tag{41}$$

The effective nucleon-nucleon interaction should be based upon a realistic nucleon-nucleon force, since our goal is to obtain a unified description of the nucleon-nucleon, nucleon-nucleus and nucleus-nucleus scattering (a discussion about the "realism" of the interaction is found in Refs. [1,6]). For instance, a realistic interaction should match the empirical values for the volume integral and root-mean-square radius of the nucleon-nucleon interaction, $V_0 \approx -430\ MeV\ fm^3$ and $r_{rms} \approx 1.5\ fm$, that were extrapolated from the main features of the optical potential for the nucleon-nucleus scattering at $E_{nucleon} = 10\ MeV$ [1,46–48]. The M3Y interaction has been derived [1] with basis on the G-matrix for two nucleons bound near the Fermi surface, and certainly is representative of realistic interactions. In table 3 are presented the volume integral and root-mean-square radius for several nucleon-nucleon interactions used in this work, including the M3Y at 10 $MeV/nucleon$.

The M3Y interaction is not truly appropriate for use in the context of the nonlocal model, because it already contains a simulation of the exchange effects included in its knock-on term. Furthermore, according to the nonlocal model the

energy-dependence of the local-equivalent potential should be related only to the finite range of the Pauli nonlocality, but the knock-on exchange term in the M3Y interaction is also energy-dependent. Therefore, the use of the M3Y in the nonlocal model would imply a double counting of the energy-dependence that arises from exchange effects. In Section 4, we have demonstrated that the LE potential is identical with the double-folding potential for energies near the barrier, which are in a region around 10 $MeV/nucleon$. In this same energy range, the folding potential with the M3Y interaction have provided a very good description of elastic scattering data for several heavy-ion systems [1]. Thus, we believe that an appropriate nucleon-nucleon interaction for the nonlocal model could be the M3Y "frozen" at 10 $MeV/nucleon$ [13], i.e. considering the parameters of the Reid and Paris versions as energy-independent values. Fig. 11 (top) shows a comparison between experimental and theoretical heavy-ion reduced potentials, in which the "frozen" M3Y-Reid was considered for the nucleon-nucleon interaction. We emphasize that no adjustable parameter has been used in these calculations, but even so a good agreement between data and theoretical prediction has been obtained. The "frozen" M3Y-Paris provides similar results.

With the aim of investigating how much information about the effective nucleon-nucleon interaction can be extracted from our heavy-ion potential systematics, we have considered other possible functional forms for this effective interaction. Besides the Yukawa function (Eq. 25), we have also used the Gaussian (Eq. 42) and the exponential (Eq. 43), which reduce to the tri-dimensional delta function in the limit $\sigma \rightarrow 0$,

$$G_\sigma(r) = V_0 \, \frac{e^{-r^2/2\sigma^2}}{(2\pi)^{3/2} \, \sigma^3} \, , \tag{42}$$

$$E_\sigma(r) = V_0 \, \frac{e^{-r/\sigma}}{8\pi\sigma^3} \, . \tag{43}$$

The fits obtained with all these functions are of similar quality and comparable with that for the M3Y interaction (Fig. 11 - top). The resulting best fit widths (σ), volume integrals and corresponding root-mean-square radii are found in table 3. All the V_0 and r_{rms} values, including those of the M3Y, are quite similar. Also the "experimentally" extracted intensity of the nucleon-nucleon interaction in the region $1 \leq r \leq 3 \; fm$ seems to be rather independent of the model assumed for this interaction (see Fig. 12).

In Section 5, we have demonstrated that the major part of the "finite-range" of the heavy-ion nuclear potential is related only to the spatial extent of the nuclei. In fact, even considering a zero-range for the interaction v_{NN} in Eq. 8, the shape of the heavy-ion potential could be well described just by folding the matter densities of the two nuclei. One would ask whether the finite-range shape of the effective nucleon-nucleon interaction can be derived in a similar way. Thus, we have considered a folding-type effective nucleon-nucleon interaction built from:

$$v_{NN}(\vec{r}) \approx v_f(r) = \int \rho_m(r_1) \, \rho_m(r_2) \, V_0 \, \delta(\vec{R} - \vec{r_1} + \vec{r_2}) \, d\vec{r_1} \, d\vec{r_2} = \frac{2\pi V_0}{r} \int_0^\infty r_1 \, \rho_m(r_1) \left[\int_{|r-r_1|}^{r+r_1} r_2 \, \rho_m(r_2) \, dr_2 \right] dr_1 \, , \tag{44}$$

where $V_0 = -456 \; MeV \; fm^3$ as determined by the heavy-ion potential analysis, and ρ_m is the matter density of the nucleon. Based on the intrinsic charge distribution of the proton in free space, which has been determined by electron scattering experiments, we have assumed an exponential shape for the matter density of the nucleon

$$\rho_m(r) = \rho_0 \, e^{-r/a_m} \, . \tag{45}$$

Of course, ρ_0 and a_m are connected by the normalization condition, Eq. 2. The integration of Eq. 44 results in

$$v_f(r) = V_0 \, \pi \, a_m^3 \, \rho_0^2 \, e^{-r/a_m} \, \left(1 + \frac{r}{a_m} + \frac{r^2}{3a_m^2} \right) \, . \tag{46}$$

With this finite-range folding-type effective nucleon-nucleon interaction, a good fit of the reduced heavy-ion potential strengths is obtained (see Fig. 11 - bottom), with realistic volume integral and root-mean-square radius (see table 3). The folding-type interaction is quite similar to both versions of the M3Y interaction in the surface region (see Fig. 12).

The folding-type interaction in the context of the nonlocal model provides a very interesting unification between the descriptions of the nucleus-nucleus, nucleon-nucleus and effective nucleon-nucleon interactions. This can be appreciated through the comparison between Eqs. 36 and 38, with the subtle detail that V_F (in Eq. 36) and v_f (in Eq. 38) can both be calculated by folding the matter densities in the zero-range approach, and with the same V_0 value. Therefore, the interaction between two nuclei (or nucleons) can be obtained from

$$V_{LE}(R) = \int \rho_1(r_1)\, \rho_2(r_2)\, V_0\, \delta(\vec{R} - \vec{r_1} + \vec{r_2})\, e^{-4v^2/c^2}\, d\vec{r_1}\, d\vec{r_2} \qquad (47)$$

where $V_0 = -456\ MeV\ fm^3$, ρ_i are the matter densities, and v is the relative speed between the nuclei (or nucleons). An alternative way to calculate the heavy-ion interaction is with the Eq. 37 (and 38), but in this case the nucleon distributions must be used (in Eq. 37) instead of the matter densities. All these findings seems to be quite consistent. However, the best fit value obtained for the diffuseness ($a_m = 0.30\ fm$) of the matter density of the nucleon inside the nucleus is considerable greater than that ($a_{chp} = 0.235\ fm$) found for the charge distribution of the proton in free space. This finding is consistent with the swelling of the nucleon observed in the EMC effect [49], but should be contrasted with the opposite picture of a smaller nucleon inside the nucleus as advanced within the concept of color transparency [50].

Finally, we mention that, if the energy-dependence of the Pauli nonlocality is not taken into account and the experimental potential strengths are associated directly with the folding potential, our calculations indicate that the corresponding effective nucleon-nucleon interaction should have the following unrealistic values: $V_0 \approx -270\ MeV\ fm^3$ and $r_{rms} \approx 1.9\ fm$.

7. Conclusion

The experimental potential strengths considered in the present systematics have been obtained at the corresponding sensitivity radii, a region where the nuclear potential is determined from the data analyses with the smallest degree of ambiguity. The Fermi distribution was assumed to represent the nuclear densities, with parameters consistent with an extensive amount of theoretical (DHB calculations) and experimental (electron scattering experiments) results. The potential data set is well described in the context of the nonlocal model, by the double-folding potential in the zero-range as well as in the finite-range approaches. The dispersion of the potential data around the theoretical prediction is 25%, which is compatible with the expected effects arising from the variation of the densities due to the structure of the nuclei. If the nonlocal interaction is assumed, the heavy-ion potential data set seems to determine a few characteristics of the effective nucleon-nucleon interaction, such as volume integral and root-mean-square radius, in a model-independent way.

The description of the bare potential presented in this work is based only on two fundamental ideas: the folding model and the Pauli nonlocality. We have avoided as much as possible the use of adjustable parameters, and in the case of the "frozen" M3Y interaction no adjustable parameters were necessary to fit the experimental potential strengths. Nowadays, the other important part of the heavy-ion interaction, the polarization potential, is commonly treated within a phenomenological approach, with several adjustable parameters which usually are energy-dependent and vary significantly from system to system. The association of the nonlocal bare potential presented in this work with a more fundamental treatment of the polarization should be the next step toward a global description of the nucleus-nucleus interaction.

This work was partially supported by Financiadora de Estudos e Projetos (FINEP), Fundação de Amparo à Pesquisa do Estado de São Paulo (FAPESP), and Conselho Nacional de Desenvolvimento Científico e Tecnológico (CNPq).

---

[1] G. R. Satchler and W. G. Love, Phys. Rep. **55**, 183 (1979).
[2] L. J. B. Goldfarb and Y. K. Gambhir, Nucl. Phys. **A401**, 557 (1983).
[3] D. M. Brink and N. Rowley, Nucl. Phys. **A219**, 79 (1974).
[4] R. A. Broglia and A. Winther, Phys. Rep. **C4**, 153 (1972).
[5] J. Blocki, J. Randrup, W. J. Swiatecki and C. F. Tsang, Ann. Phys. **105**, 427 (1977).
[6] M. E. Brandan and G. R. Satchler, Phys. Rep. **285**, 142 (1997), and references therein.
[7] P. R. Christensen and A. Winther, Phys. Lett. **B65**, 19 (1976).
[8] C. P. Silva, M. A. G. Alvarez, L. C. Chamon, D. Pereira, M. N. Rao, E. S. Rossi Jr., L. R. Gasques, M. A. E. Santo, R. M. Anjos, J. Lubian, P. R. S. Gomes, C. Muri, B. V. Carlson, S. Kailas, A. Chatterjee, P. Singh, A. Shivastava, K. Mahata and S. Santra, Nucl. Phys. **A679**, 287 (2001).
[9] D. A. Goldberg and S. M. Smith, Phys. Rev. Lett. **29**, 500 (1972).
[10] D. A. Goldberg and S. M. Smith, Phys. Rev. Lett. **33**, 715 (1974).
[11] D. A. Goldberg, S. M. Smith and G. F. Burdzic, Phys. Rev. **C10**, 1362 (1974).

[12] M. A. C. Ribeiro, L. C. Chamon, D. Pereira, M. S. Hussein and D. Galetti, Phys. Rev. Lett. **78**, 3270 (1997).
[13] L. C. Chamon, D. Pereira, M. S. Hussein M. A. C. Ribeiro and D. Galetti, Phys. Rev. Lett. **79**, 5218 (1997).
[14] L. C. Chamon, D. Pereira and M. S. Hussein, Phys. Rev. **C58**, 576 (1998).
[15] H. De Vries, C. W. De Jager and C. De Vries, Atomic Data and Nucl. Data Tables **36**, 495 (1987).
[16] E. G. Nadjakov, K. P. Marinova and Y. P. Gangrsky, Atomic Data and Nucl. Data Tables **56**, 133 (1994).
[17] B. V. Carlson and D. Hirata, Phys. Rev. **C62**, 054310 (2000).
[18] G. A. Lalazissis, J. König and P. Ring, Phys. Rev. **C57**, 540 (1997).
[19] G. A. Lalazissis, D. Vretenar and P. Ring, Phys. Rev **C57**, 2294 (1998).
[20] G. A. Lalazissis, D. Vretenar, P. Ring, M. Stoitsov and L. Robledo, Phys. Rev. **C60**, 014310 (1999).
[21] W. D. Myers, Nuc. Phys. **A204**, 465 (1973).
[22] G. R. Satchler, Phys. Rep. **199**, 147 (1991).
[23] F. Perey and B. Buck, Nucl. Phys. **32**, 253 (1962).
[24] T. H. R. Skyrme, Philos. Mag. **1**, 1043 (1956).
[25] G. Ripka, Nucl. Phys. **42**, 75 (1963).
[26] W. Bauhoff, H. V. von Geramb and G. Palla, Phys. Rev. **C27**, 2466 (1983).
[27] W. E. Frahn and R. H. Lemmer, Nuovo Cimento **5**, 1564 (1957).
[28] D. F, Jackson and R. C. Johnson, Phys. Lett. **B49**, 249 (1974).
[29] F. Lenz and E. J. Moniz, Phys. Rev. **C12**, 909 (1975).
[30] L. C. Chamon, D. Pereira, E. S. Rossi Jr., C. P. Silva, R. Lichtenthaler Filho and L. C. Gomes, Nucl. Phys. **A582**, 305 (1995).
[31] L. C. Chamon, D. Pereira, E. S. Rossi Jr., C. P. Silva, H. Dias, L. Losano and C. A. P. Ceneviva, Nucl. Phys. **A597**, 253 (1996).
[32] M. A. G. Alvarez, L. C. Chamon, D. Pereira, E. S. Rossi Jr., C. P. Silva, L. R. Gasques, H. Dias and M. O. Roos, Nucl. Phys. **A656**, 187 (1999).
[33] E. S. Rossi Jr., L. C. Chamon, D. Pereira, C. P. Silva and G. Ramirez, J. Phys. **G23**, 1473 (1997).
[34] M. Ermer, H. Clement, G. Frank, P. Grabmayr, H. Heberle and G. J. Wagner, Phys. Lett. **B224**, 40 (1989).
[35] A. Nadasen, T. Stevens, J. Farhat, J. Brusoe, P. Schwandt, J. S. Winfield, G. Yoo, N. Anantaraman, F. D. Becchetti, J. Brown, B. Hotz, J. W. Janecke, D. Roberts and R. E. Warner, Phys. Rev. **C47**, 674 (1993).
[36] A. Nadasen, M. McMaster, G. Gunderson, A. Judd, S. Villanueva, P. Schwandt, J. S. Winfield, J. van der Plicht, R. E. Warner, F. D. Becchetti and J. W. Janecke, Phys. Rev. **C37**, 132 (1988).
[37] A. Nadasen, M. McMaster, M. Fingal, J. Tavormina, P. Schwandt, J. S. Winfield, M. F. Mohar, F. D. Becchetti, J. W. Janecke and R. E. Warner, Phys. Rev. **C39**, 536 (1989).
[38] A. Nadasen, J. Brusoe, J. Farhat, T. Stevens, J. Williams, L. Nieman, J. S. Winfield, R. E. Warner, F. D. Becchetti, J. W. Janecke, T. Annakkage, J. Bajema, D. Roberts and H. S. Govinden, Phys. Rev. **C52**, 1894 (1995).
[39] H. G. Bohlen, M. R. Clover, G. Ingold, H. Lettau and W. von Oertzen, Z. Phys. **A308**, 121 (1982).
[40] M. Buenerd, A. Lounis, J. Chauvin, D. Lebrun, P. Martin, G. Duhamel, J. C. Gondrand and P. de Saintignon, Nucl. Phys. **A424**, 313 (1984).
[41] J. Y. Hostachy, M. Buenerd, J. Chauvin, D. Lebrun, Ph. Martin, J. C. Lugol, L. Papineau, P. Roussel, N. Alamanos, J. Arvieux and C. Cerruti, Nucl. Phys. **A490**, 441 (1988).
[42] P. Roussel-Chomaz, N. Alamanos, F. Auger, J. Barrete, B. Berthier, B. Fernandez, L. Papineau, H. Doubre and W. Mittig, Nucl. Phys. **A477**, 345 (1988).
[43] G. Bartnitzky, A. Blazevic, H. G. Bohlen, J. M. Casandjian, M. Chartier, H. Clement, B. Gebauer, A. Gilibert, Th. Kirchner, Dao T. Khoa, A. Lepine-Szily, W. Mittig, W. von Oertzen, A. N. Ostrowski, P. Roussel-Chomaz, J. Siegler, M. Wilpert and Th. Wilpert, Phys. Lett. **B365**, 23 (1996).
[44] F. Nuoffer, G. Bartnitzky, H. Clement, A. Blazevic, H. G. Bohlen, B. Gebauer, W. von Oertzen, M. Wilpert, T. Wilpert, A. Lepine-Szily, W. Mittig, A. N. Ostrowski and P. Roussel-Chomaz, Il Nuovo Cimento **A11**, 971 (1998).
[45] N. Alamanos, F. Auger, J. Barrete, B. Berthier, B. Fernandez, J. Gastebois, L. Papineau, H. Doubre and W. Mittig, Phys. Lett. **B137**, 37 (1984).
[46] F. D. Bechetti and G. W. Greenlees, Phys. Rev. **182**, 1190 (1969).
[47] G. W. Greenlees, G. J. Pyle and Y. C. Yang, Phys. Rev. **171**, 1115 (1968).
[48] G. W. Greenlees, W. Makofske and G. J. Pyle, Phys. Rev **C1**, 1145 (1970).
[49] J. J. Aubert *et al.*, Phys. Lett. **B123**, 275 (1983).
[50] See, e.g., L. L. Frankfurt and M. I. Strikman, Phys. Rep. **76**, 214 (1981); **160**, 235 (1988).

Table 1: The table presents the systems, sub-barrier bombarding energies, and corresponding references, that have been included in the nuclear potential systematics.

System	E_{Lab} (MeV)	Reference
$^{16}O + ^{58}Ni$	35, 35.5, 36, 36.5, 37, 38	[8,31]
$^{16}O + ^{60}Ni$	35, 35.5, 36, 37, 38	[30,31]
$^{16}O + ^{62,64}Ni$	34, 35, 36	[31]
$^{16}O + ^{88}Sr$	43, 44, 45	[32]
$^{16}O + ^{90}Zr$	46, 47, 48	[32]
$^{16}O + ^{92}Zr$	45, 46, 47, 48	[8,32]
$^{16}O + ^{92}Mo$	48, 48.5, 49	[32]
$^{16}O + ^{120}Sn$	53, 54, 55	[8]
$^{16}O + ^{138}Ba$	54, 55, 56, 57	[8]
$^{16}O + ^{208}Pb$	74, 75, 76, 77, 78	[8]
$^{18}O + ^{58}Ni$	35.1, 35.5, 37.1, 38	[33]
$^{18}O + ^{60}Ni$	34.5, 35.5, 37.1, 38	[33]

Table 2: The same of table 1, but for intermediate energies.

System	E_{Lab} (MeV)	Reference
$p + ^{40}Ca, ^{208}Pb$	30.3	[34]
$d + ^{40}Ca, ^{208}Pb$	52	[34]
$^{4}He + ^{40}Ca, ^{208}Pb$	104	[34]
$^{6}Li + ^{12}C, ^{28}Si$	210, 318	[35,36]
$^{6}Li + ^{40}Ca, ^{58}Ni, ^{90}Zr, ^{208}Pb$	210	[37]
$^{7}Li + ^{12}C, ^{28}Si$	350	[38]
$^{12}C + ^{12}C$	300, 360, 1016, 1440, 2400	[39–41]
$^{12}C + ^{208}Pb$	1440	[41]
$^{13}C + ^{208}Pb$	390	[40]
$^{16}O + ^{16}O$	250, 350, 480, 704, 1120	[43,44]
$^{16}O + ^{12}C, ^{28}Si, ^{40}Ca, ^{90}Zr, ^{208}Pb$	1504	[42]
$^{40}Ar + ^{60}Ni, ^{120}Sn, ^{208}Pb$	1760	[45]

Table 3: The width, volume integral and root-mean-square radius for several effective nucleon-nucleon interactions considered in this work.

Interaction	σ or a_m (fm)	V_0 $(MeV\ fm^3)$	r_{rms} (fm)
M3Y-Reid	-	- 408	1.62
M3Y-Paris	-	- 447	1.60
Yukawa	0.58	- 439	1.42
Gaussian	0.90	- 448	1.56
Exponential	0.43	- 443	1.49
Folding-type	0.30	- 456	1.47

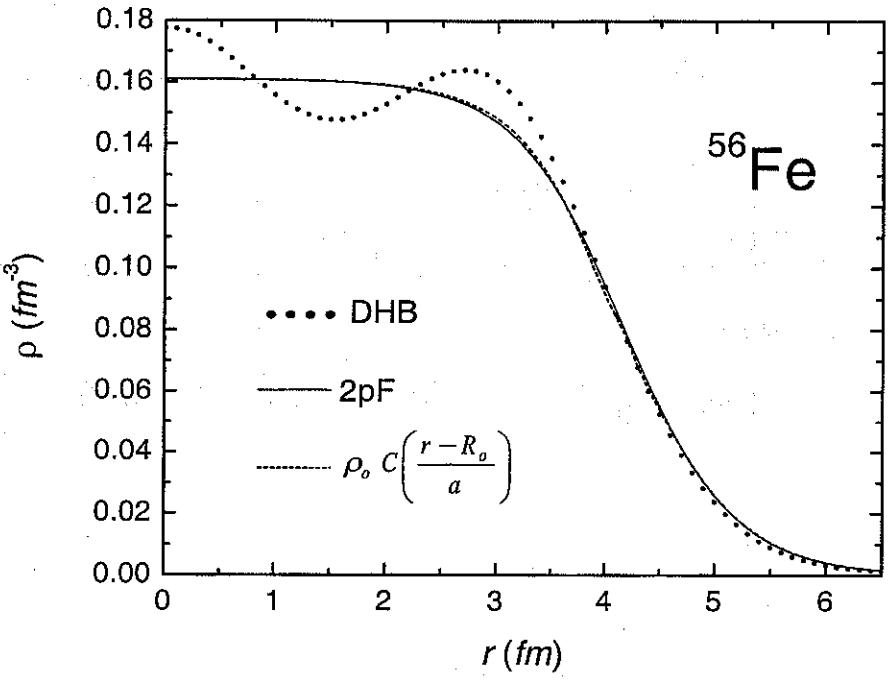

FIG. 1. Nucleon density for the ^{56}Fe nucleus represented through Dirac-Hartree-Bogoliubov calculations (DHB) and a two-parameter Fermi distribution (2pF), with $a = 0.5\ fm$ and $R_0 = 4.17\ fm$. The small difference between the 2pF distribution and the function $\rho_0\ C\left(\frac{r-R_0}{a}\right)$ (Eqs. 12, 13 and 14) is hardly seen in the figure.

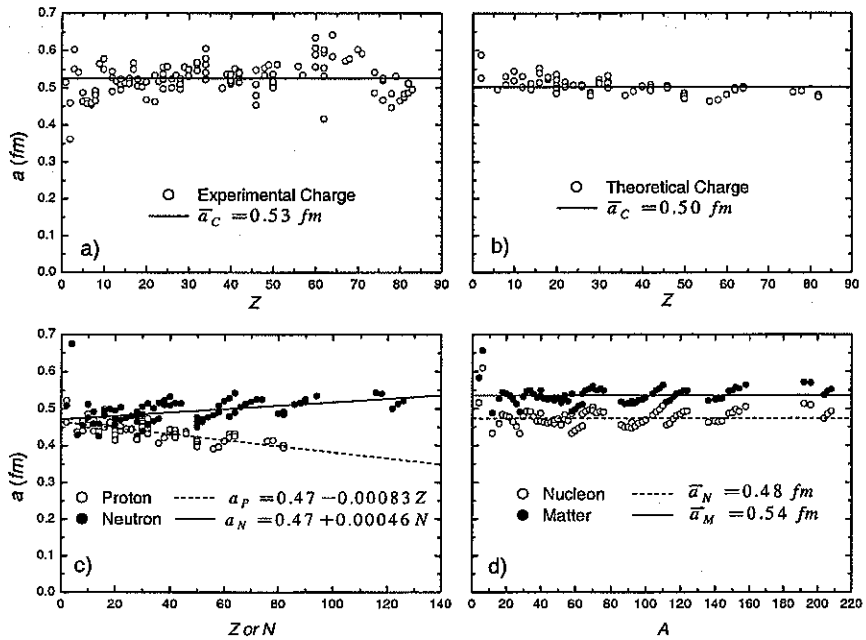

FIG. 2. Equivalent diffuseness values obtained for charge distributions extracted from electron scattering experiments and for theoretical densities obtained from Dirac-Hartree-Bogoliubov calculations.

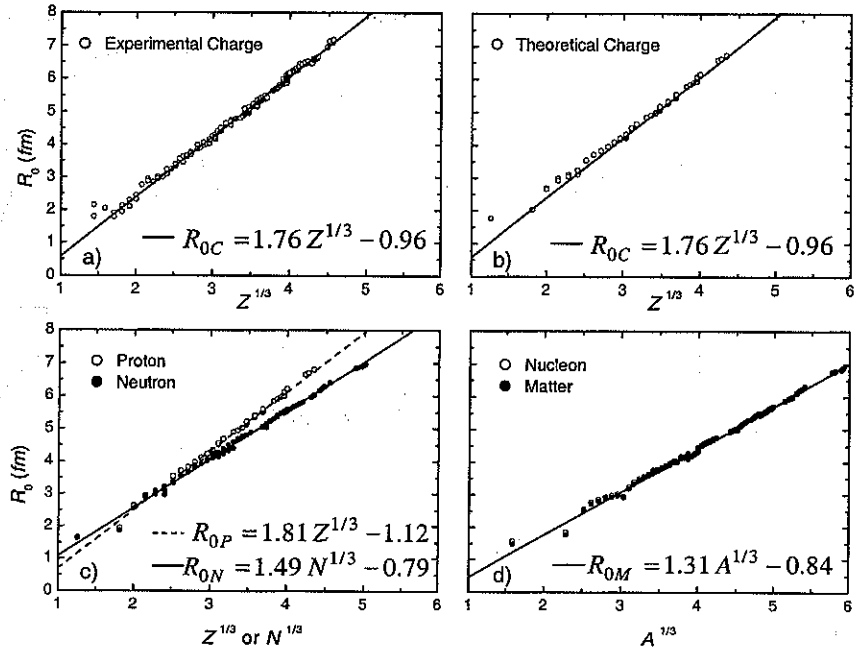

FIG. 3. The R_0 parameter obtained for charge distributions extracted from electron scattering experiments and for theoretical densities obtained from Dirac-Hartree-Bogoliubov calculations.

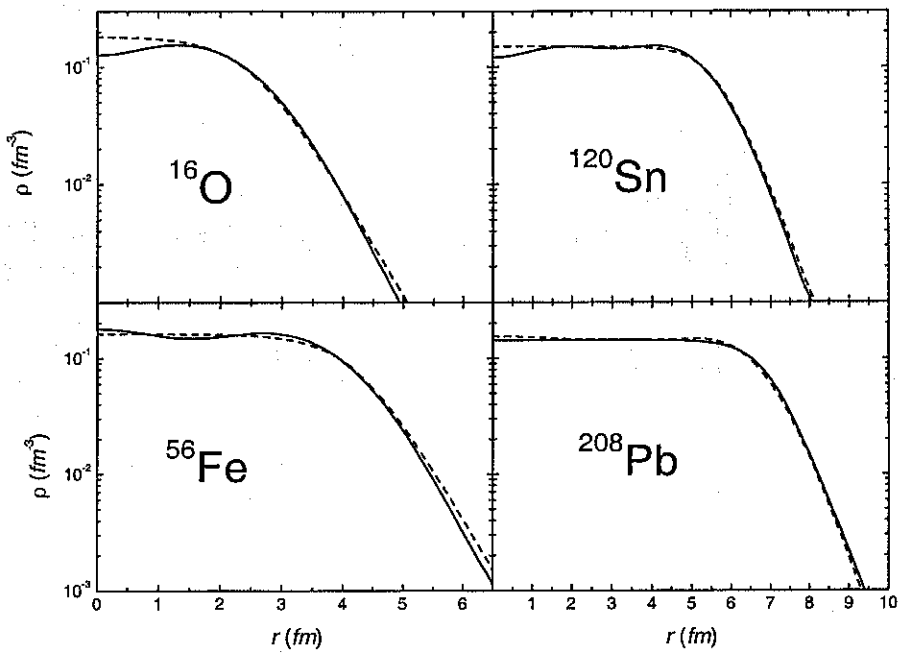

FIG. 4. Nucleon densities from Dirac-Hartree-Bogoliubov calculations (solid lines) compared with the corresponding two-parameter Fermi distributions (dashed lines), with $a = 0.50\ fm$ and R_0 obtained through Eq. 6.

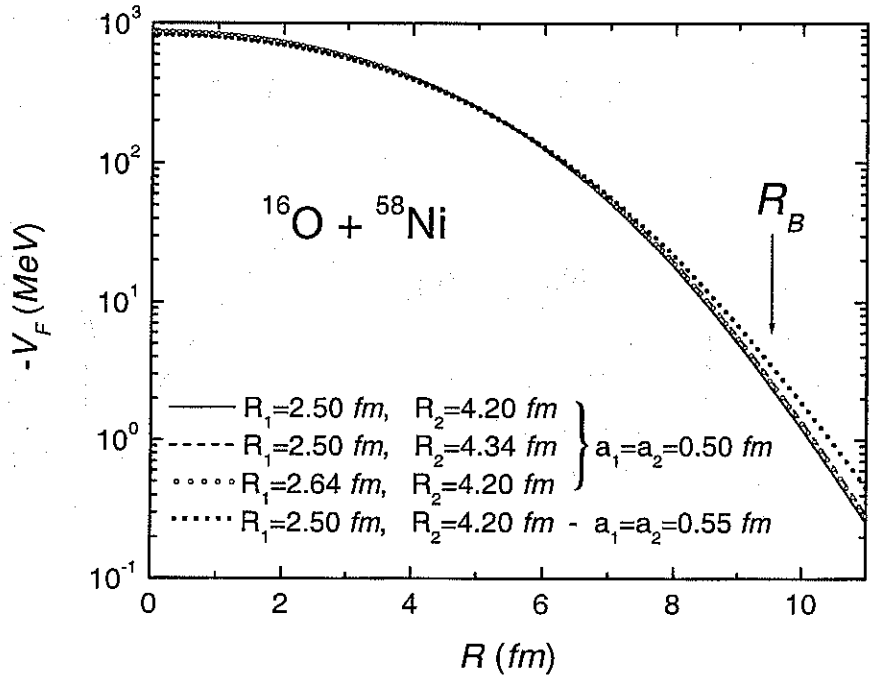

FIG. 5. Folding potential for different sets of 2pF densities that may represent the $^{16}O + ^{58}Ni$ system. The approximate position of the s-wave barrier radius (R_B) is indicated in the figure.

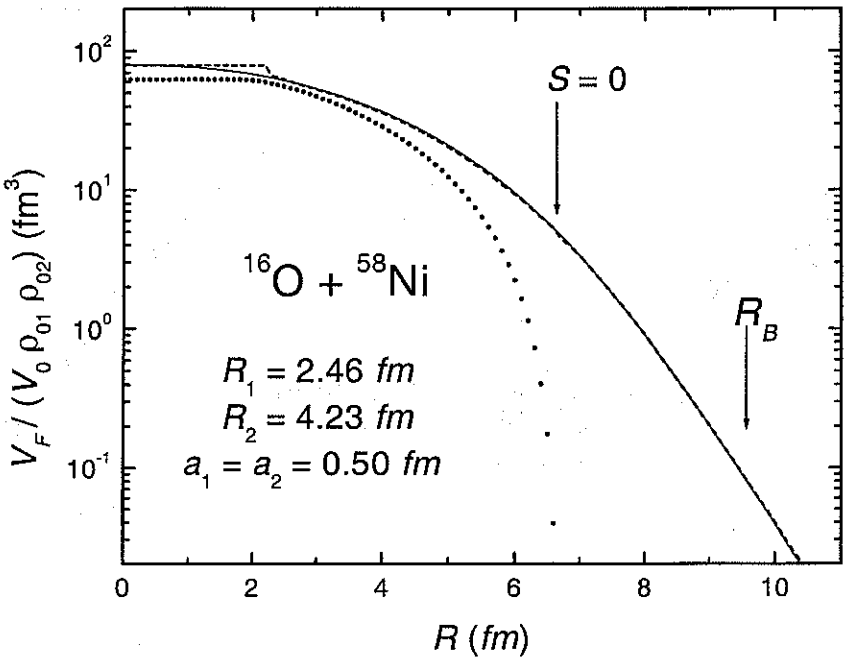

FIG. 6. Folding potential in the zero-range approach calculated from numerical integration of Eq. 8 (solid line), for 2pF densities that may represent the $^{16}O + ^{58}Ni$ system. The dashed line represents the approximate analytical expressions, Eqs. 15, 16 and 17, while the dotted line concerns the exact result for $a = 0$, Eqs. 9, 10 and 11. The approximate position of the s-wave barrier radius (R_B) and of the distance $R = R_1 + R_2$ ($s = 0$) are indicated in the figure.

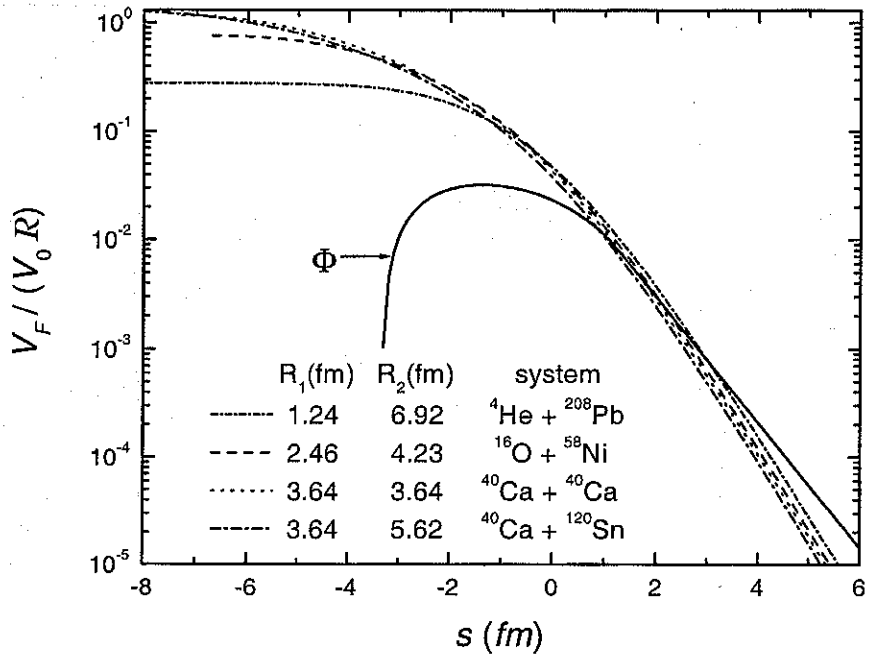

FIG. 7. Normalized folding potential $V_F/(V_0\mathcal{R})$ in the zero-range approach (Eq. 8) as a function of the distance $s = R - (R_1 + R_2)$, for several sets of 2pF distributions (with $a = 0.50\ fm$) that may represent the systems indicated in the figure. The proximity universal function Φ is also presented in arbitrary units.

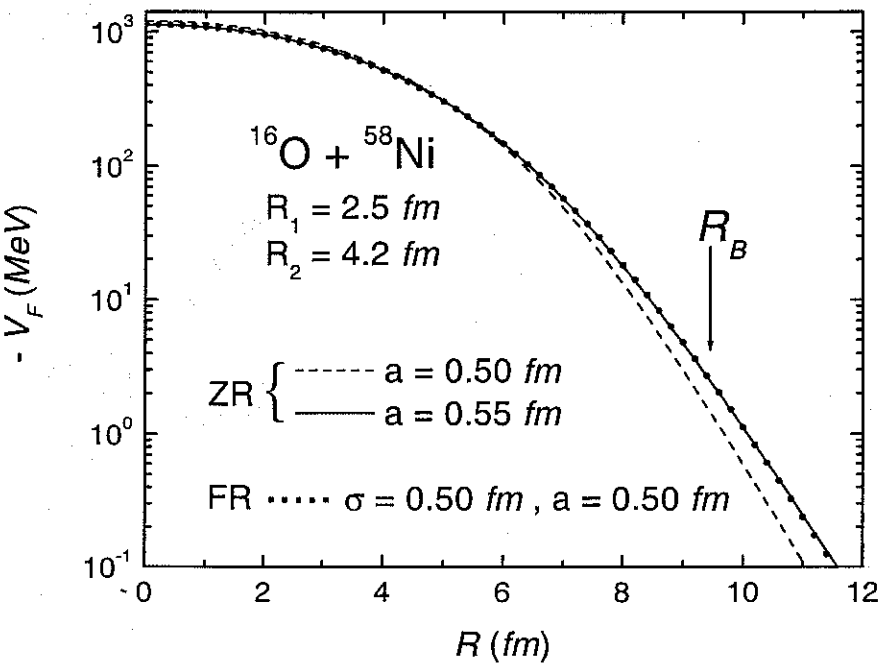

FIG. 8. Double-folding potentials for 2pF distributions with different diffuseness values (a) that may represent the ^{16}O + ^{58}Ni system. The potentials have been calculated in the zero-range approach (ZR) or with a finite-range (FR) Yukawa function for the effective nucleon-nucleon interaction.

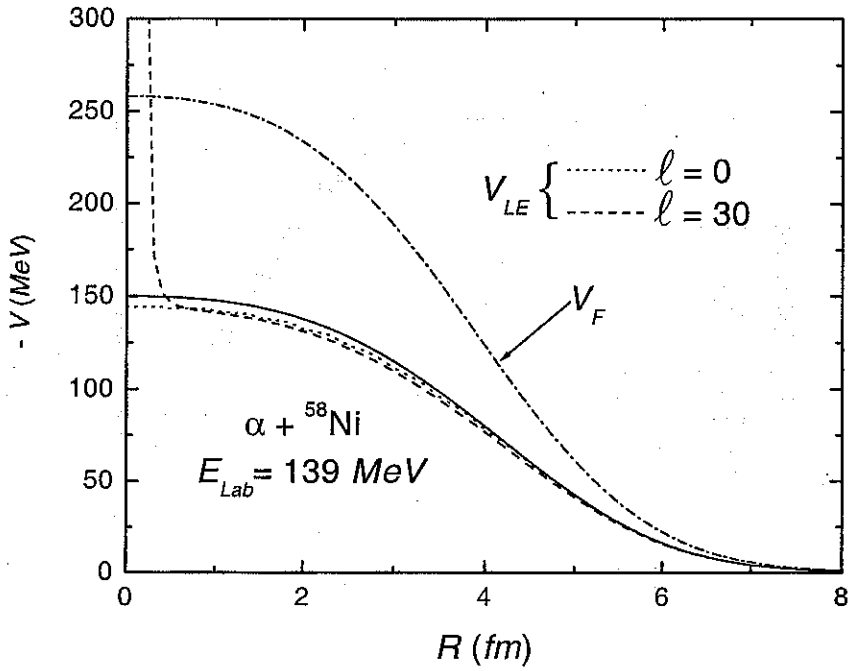

FIG. 9. Double-folding (V_F) and ℓ-dependent local-equivalent (V_{LE}) potentials for the $\alpha + {}^{58}$Ni system at $E_{Lab} = 139\ MeV$. The solid line represents the approximate expression, Eq. 34, for the local-equivalent potential.

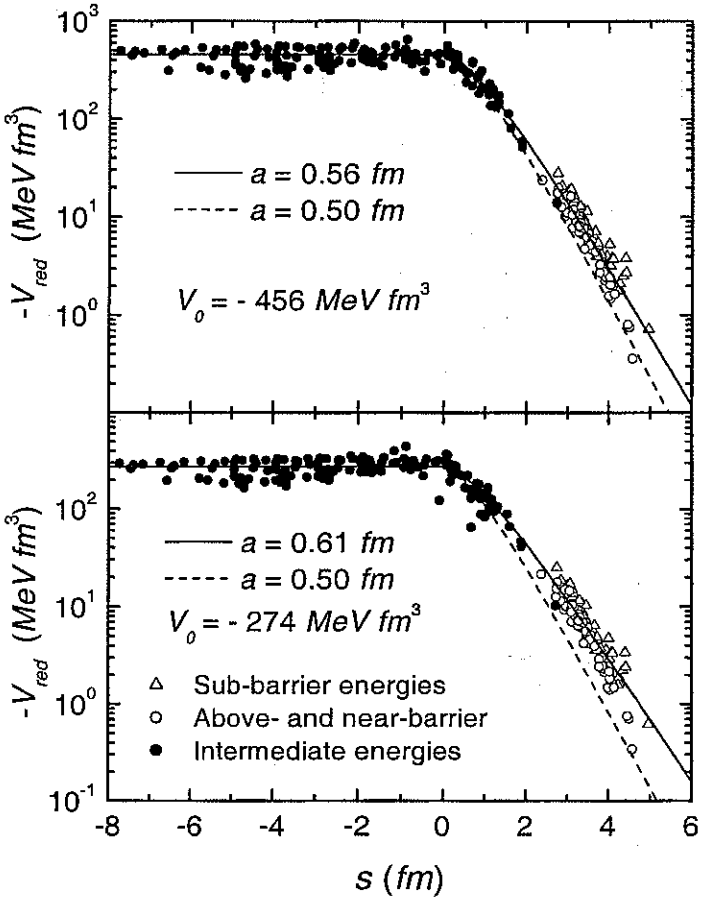

FIG. 10. Experimental and theoretical reduced potentials in the context of the zero-range approach, with (top) or without (bottom) considering in the calculations the energy-dependence of the local-equivalent potential (Eq. 34) that arises from the Pauli nonlocality.

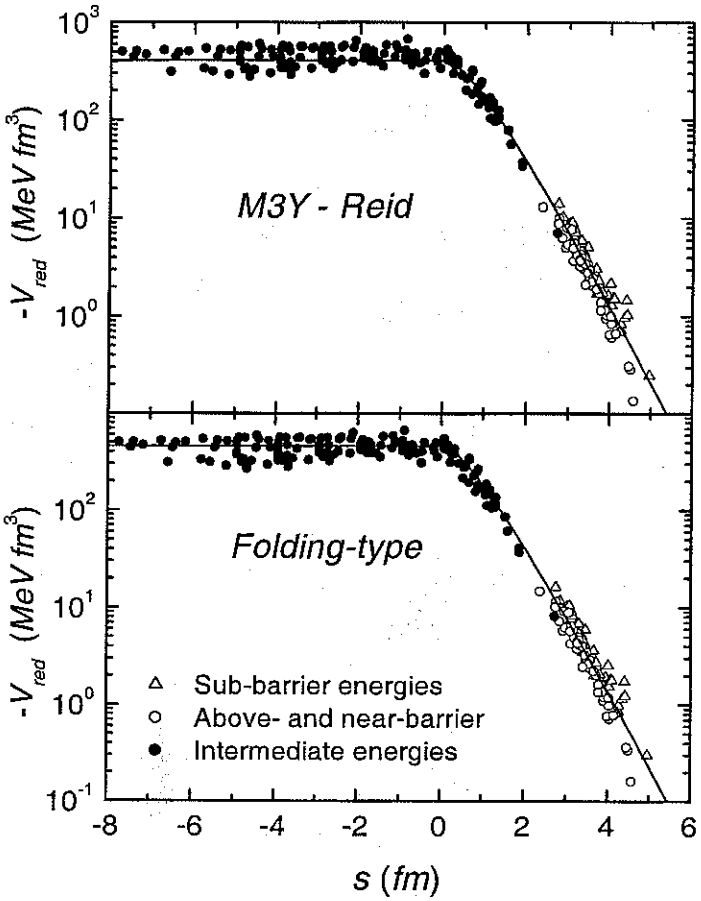

FIG. 11. Comparison between experimental and theoretical reduced potentials in the context of the finite-range approach, with a M3Y-Reid (top) or folding-type (bottom) effective nucleon-nucleon interaction.

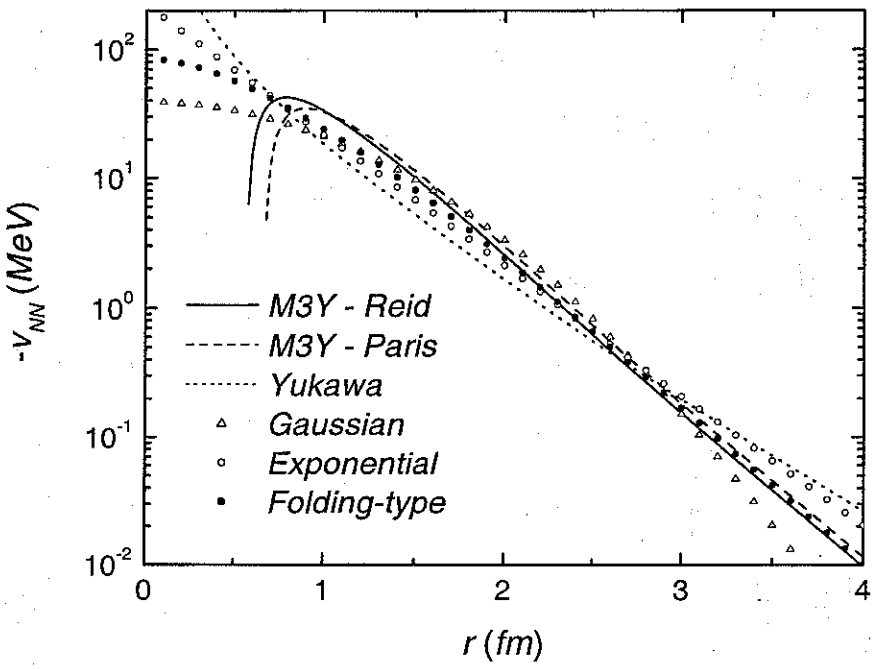

FIG. 12. The complete set of effective nucleon-nucleon interactions considered in this work.